Optics Letters

Dual stage fiber amplifier operating near 3 μm with milijoule-level, sub-ns pulses at 5 W

Yiğit Ozan Aydin,[1,2,*] Sébastien Magnan-Saucier,[1] Daiying Zhang,[2] Vincent Fortin,[1] Darren Kraemer,[2] Réal Vallée,[1] and Martin Bernier[1]

[1]Centre d'Optique, Photonique et Laser (COPL), Université Laval, Québec, Québec G1V 0A6, Canada
[2]Light Matter Interaction Inc., 88 Advance Rd., Toronto, Ontario M8Z 2T7, Canada
*Corresponding author: yoayd@ulaval.ca

Received 14 June 2021; revised 8 August 2021; accepted 10 August 2021; posted 11 August 2021 (Doc. ID 434182); published 7 September 2021

We report a 2800 nm Er^{3+}-doped fluoride fiber amplifier that delivers 1 mJ pulses with an average power of 5 W and pulse duration of 1 ns at 5 kHz repetition rate. To the best of our knowledge, this is the highest pulse energy achieved from a fluoride-fiber-based system operating near 3 μm, and the W-level average power and short pulse lengths make the system a promising tool for biomaterials processing.

https://doi.org/10.1364/OL.434182

Fluoride fiber lasers operating near 3 μm have experienced increased interest in the last decade as they reached important milestones in both CW and pulsed regimes. This progress has been fueled by advances in fiber-based components [e.g., fiber Bragg gratings, splices, and pump combiners (PCs)] and the potential clinical applications of these laser sources in medicine. It is the absorption peak of water located near 2.9 μm that allows such lasers to efficiently address different biomedical processing applications, namely, in dentistry, osteotomy, and dermatology [1–3]. Er:YAG solid state lasers have utility as a clinical tool due to their high gain at 2.94 μm, their capability of pulse modulation, and their ability to generate joule-level pulse energy. However, such bulk lasers are capable of producing pulses only from tens of nanoseconds to the microsecond range, which are not short enough to achieve confinement of acoustic energy on the targeted biomaterial volume. In this situation, the processing efficiency of the tissue diminishes, and energy diffusion produces collateral injuries bordering the incisions. To minimize these drawbacks, it is essential to use pulse durations of ≤ 1 ns where confinement of both thermal and acoustic energy is obtained [4,5].

Optical parametric generators (OPGs) are an alternative source to conventional gain materials for generating ≤ 1 ns pulses around 2.9 μm. Nevertheless, the size and complexity of these systems increase significantly with their output average power. Due to recent developments in soft-glass technology and components, fluoride fiber laser systems now provide a compact, efficient, and reliable solution to generate high-power laser radiation near 3 μm without critical alignment [6,7]. Various fluoride fiber laser configurations have been recently demonstrated to produce short pulses based on conventional techniques such as *Q*-switching and mode-locking with Er^{3+}- or Ho^{3+}-doped fibers. The pulse duration obtained with a *Q*-switched laser cavity is typically in the tens to hundreds of nanoseconds range, which is significantly longer than the thermal relaxation time of biomaterials. Recently, a pulse duration of 13 ns, which is the shortest ever produced from a *Q*-switched fluoride fiber laser, was obtained by Shen *et al*. with a mW-level average power [8]. Mode-locked fluoride laser cavities (using various saturable absorbers or nonlinear polarization evolution) have also been reported to produce shorter pulses. However, the pulse energy of these MHz-range laser cavities is generally limited to the nJ-level [9]. In addition to further amplification, the repetition rate must be reduced for tissue processing, to avoid local accumulation of heat due to a lack of diffusion time between pulses [10]. Hence, one of the most efficient ways to produce high pulse energy, high average power, and short pulse duration, all together near 3 μm, is with a hybrid approach relying on fluoride fiber amplifiers seeded by a compact OPG source.

Erbium-doped zirconium fluoride (Er^{3+}:ZrF_4) fibers are ideal media for 3 μm laser generation due to their broad emission band extending from 2.7 to 3 μm, and their convenient pumping (absorption) band, overlapping with commercially available InGaAs laser diodes between 940 and 980 nm. The amplification near 3 μm relies on the erbium transition $^4I_{11/2} \rightarrow {}^4I_{13/2}$. Based on this approach, watt-level amplification near 3 μm from an Er^{3+}:ZrF_4 gain has been successfully demonstrated in the CW regime [11,12]. In short-pulse regimes, OPG seeded amplification has been studied to obtain high pulse energy levels. In one demonstration, 24-ps-long pulses with 84 μJ energy were obtained from an OPA seeded Er:ZBLAN fiber, while the average power was limited to 0.84 W [13]. In 2018, a short-pulse amplification scheme was demonstrated by using both Er^{3+}:ZrF_4 and Ho^{3+}, Pr^{3+}:ZrF_4 fibers as gain media and a sub-ns OPG source as a seed [14]. Up to 2.45 W average power at 2.8 μm with 122 μJ pulse energy was achieved from this system, but a geometry mismatch between the fibers and free-space pumping led to fiber tip failure and power instabilities during long-term operation. More recently, Du *et al*. reported an amplifier seeded by a $KTiOAsO_4$-based OPA and achieved a

pulse energy of 0.67 mJ, 11.5 ns pulses at 2.72 μm from a 70 μm Er:ZBLAN fiber [15]. While the system has a promising pulse energy, the laser average power was limited to 7 mW.

Thus far, the lack of reliable components operating in the mid-infrared (mid-IR) region have hindered the achievement of high-energy-level pulses with short duration in fluoride-fiber-based laser systems. While amplification of short pulses to high energy within small fibers is limited by nonlinear effects, W-level average power creates additional challenges from thermal and OH-related fiber-tip limitations [16]. Today, access to high-quality fluoride fibers, high-power mid-IR isolators, and high-power fluoride fiber PCs has finally enabled the development of efficient fluoride fiber amplifiers. In this work, mJ-level pulses from a fluoride-fiber-based laser amplifier are reported for the first time. The combination of mJ pulse energy with pulse duration of only 1 ns and high average power operating at a wavelength near the fundamental OH resonance is an important development for ultrafast mid-IR sources and their eventual use in the clinical environment.

The experimental setup of the laser amplifier is shown in Fig. 1. The seed signal is generated by an optical parametric amplifier (OPA) developed by www.lightmatterinteraction.com Light Matter Interaction Inc. It consists of a periodically poled lithium niobate nonlinear crystal pumped with a 1064 nm passively Q-switched laser at a repetition rate of 5 kHz and generates ∼1 ns pulses at a central wavelength of 2.79 μm with 90 mW of average power. The amplifier is made of two stages based on 7 mol.% Er^{3+}-doped double-clad fibers with different core sizes provided by Le Verre Fluoré. All the ZrF_4-based fibers used in the system have a core numerical aperture (NA) of 0.12. The inner cladding of the fibers is coated with low-index fluoroacrylate polymer to allow pump guiding with an NA > 0.46. The core size for both stages (first: 85/250 μm, second: 115/350 μm) was chosen large enough to increase the damage threshold of the fiber and to reduce the nonlinear effects, while the cladding size was chosen to maintain a fixed core-to-cladding ratio. Optimal Er^{3+}:ZrF_4 fiber lengths were evaluated to 1.9 and 1.7 m for the first and second amplification stages, respectively. The optimization of the amplifier length was performed based on the cladding pump absorption, but also with the aim of reducing the buildup of parasitic lasing and spectral broadening through nonlinear effects.

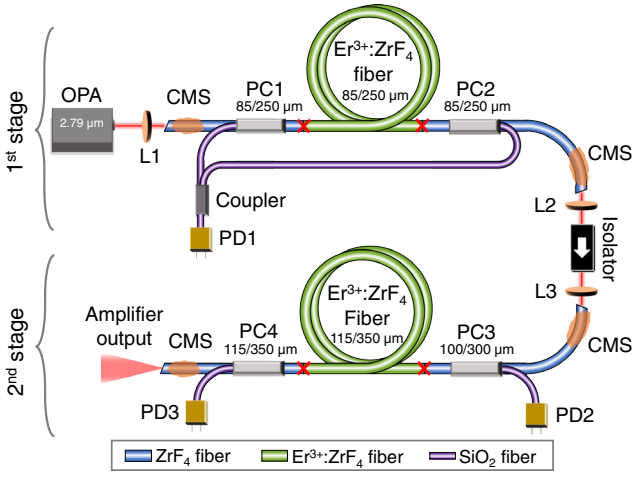

Fig. 1. Experimental setup of the laser amplifier: PD1-PD2-PD3, pump diodes; PC1-PC2-PC3-PC4, pump combiners; L1-L2-L3, ZnSe aspheric lenses; CMS, cladding mode stripper; X, splice.

The Er^{3+}:ZrF_4 fibers in the first (85/250 μm) and second amplification stages (115/350 μm) are pumped from both sides by using (1 + 1) × 1 side-PCs. These PCs are made in-house with undoped fluoride fibers matching the geometry of the doped fibers to mitigate splicing losses. More specifically, PC1 and PC2 are both made of 85/250 μm fibers, PC3 is made of a 100/300 μm fiber, whereas PC4 is fabricated from a 115/350 μm fiber. All PCs were fabricated by wrapping silica fibers around undoped ZrF4 fibers, using the method described in [17]. The pump fibers of the combiners are standard 105/125 μm multimode silica fibers with a NA of 0.22. The combiners are then spliced to the Er^{3+}:ZrF_4 fibers using a fiber splicer (Thorlabs Vytran GPX-3800) equipped with an iridium filament with splice losses estimated to less than 0.2 dB. An optical isolator made of YVO_4 (Faraday Photonics ISO-5-2800-MP) was placed between both amplification stages to avoid parasitic lasing that might cause instability in the system as the output pulse energy increases. For the same reason, the fiber tips of both input and output ends (of both stages) were cleaved at ∼6° to reduce feedback from Fresnel reflections.

Since the gain fibers have a high doping concentration and large core size, pumping near the absorption peak of the Er^{3+}-doped medium leads to high thermal loads on both ends of the doped fiber segments. Thus, we used pump diodes centered around 940 and 960 nm, whereas the absorption is much lower than the standard pumping wavelength of 976 nm, therefore reducing the heat load along the fiber. The absorption coefficients for both gain fibers are estimated to 2.4 and 4.1 dB/m for 940 and 960 nm wavelengths, respectively. The first stage is pumped by a near-IR InGaAs diode operating at approximately 940 nm (BWT K940FA5RN) and delivering up to 70 W in a 105/125 μm, 0.22 NA, silica fiber. The output of the diode is divided into two ports (also 105/125 μm) by using a 1 × 2 multimode coupler with 50/50 coupling ratio (Lightel, MMC-12-A-50-50). Then, output ports of this coupler are spliced to the combiners (PC1 and PC2) to pump the gain fiber simultaneously and at the same power level. In the second stage, pumping is provided by two 60 W InGaAs diodes (BWT K960EA5R) operating around 960 nm, also pigtailed with similar 105/125 μm fibers. The gain fibers were passively cooled by placing them on an aluminum plate. In addition, the Er^{3+}:ZrF_4 fibers were observed with a thermal imaging camera (Jenoptik, Variocam) during amplifier operation to ensure that the maximum temperature at any location did not exceed 90°C. A high-index UV-cured acrylate ($n = 1.54$) was applied to the input and output of both amplification stages to remove the unabsorbed pump coming from both backward and forward sides.

The collimated output of the OPA system is launched in PC1 through a ZnSe aspheric lens (L1, $f = 25$ mm) with an efficiency of 40%, which corresponds to 35 mW of average power and 7 μJ pulse energy. The seed signal in the first amplification stage is amplified up to 2.64 W with an efficiency of 8.4% with respect to the absorbed pump power at 940 nm. The amplified signal from the output of the first amplification stage is then collimated by using another ZnSe aspheric lens (L2, $f = 12.7$ mm) and launched to the input fiber of PC3 through another ZnSe aspheric lenses (L3, $f = 12.7$ mm). The launching efficiency from first to second amplification stage is around

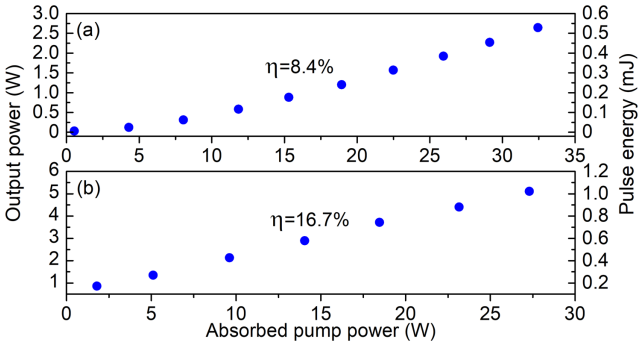

Fig. 2. Measured output power with respect to absorbed pump power after (a) first and (b) second amplification stages with first stage operating at maximum power.

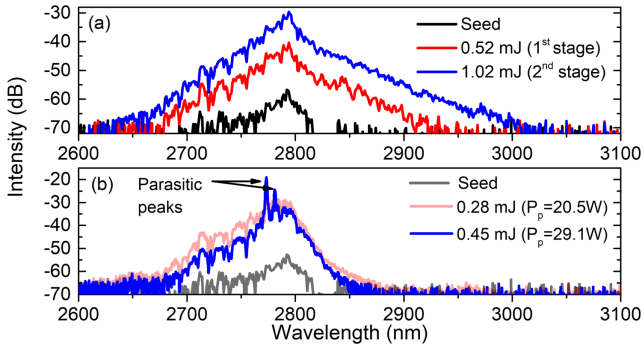

Fig. 3. (a) Spectrum of the seed source (black) and evolution of the spectrum with first (red) and second (blue) amplification stages at their maximum output energy; (b) spectrum of the seed source (black) and spectra of amplified signal with (blue) and without (red) parasitic lasing from output of first stage.

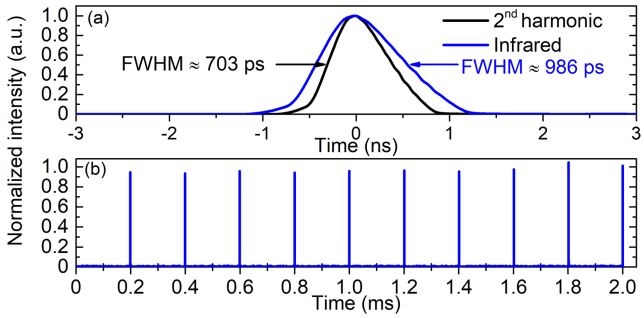

Fig. 4. (a) Pulse profile of the amplified signal and (b) measured output pulse train.

29% including lenses and isolator losses, which corresponds to 760 mW of injected signal. Since the polarization at the output of the first stage is essentially random, the polarization dependent optical isolator is the main contributing factor for such low transmission efficiency. In the second stage, 760 mW of launched signal from the first stage is amplified up to 5.1 W with an efficiency of 16.7% with respect to the absorbed pump power by simultaneously pumping both fiber ends at 960 nm at similar pump power levels. Figures 2(a) and 2(b) show the output power and output energy at 2.8 μm as a function of absorbed pump power for both amplification stages, monitored with a thermopile detector (Gentec UP19K-50F-W5-D0). The peak power at maximum pulse energy (1.02 mJ) is calculated to be ∼1 MW, and peak laser intensity in the output fiber core is estimated to be 10 GW/cm^2.

The output spectrum is characterized after each amplification stage using a mid-IR optical spectrum analyzer (Yokogawa, AQ6376, not purged) as shown in Fig. 3(a). The center wavelength of the amplified signal is at 2.79 μm and broadens compared to the seed spectrum since the Er^{3+}:ZrF_4 fiber acts as a nonlinear medium at high peak power. Most of the spectrum's energy is located between 2.7 and 3 μm where the water vapor absorption is strong. The onset of spectral broadening is also an indication that the amplifier system is operating without any parasitic laser signal. An example of an amplified spectrum exhibiting parasitic laser emission is shown in Fig. 3(b). For this measurement, the output fiber of the first amplification stage is cleaved at 0° and the Er^{3+}:ZrF_4 fiber is pumped from both sides with 940 nm diodes. As shown in Fig. 3(b), the spectral broadening is occurring after amplification of the seed signal, up to 0.28 mJ at the output of the first stage. However, as we amplify the seed signal up to 0.45 mJ, spectral broadening is stopped and CW laser peaks are observed.

The pulse temporal profile at maximum pulse energy was characterized with an InGaAs ultrafast Ge-based photo diode (Alphalas UPD-100-IR1-P, rise time <100 ps) connected to a 10 GHz bandwidth oscilloscope (Agilent Infiniium DSO81004A). Since the spectral range of the detector (400–2000 nm) does not cover the laser wavelength, the pulse temporal trace is obtained from the second harmonic signal generated by focusing the amplified signal into a BBO nonlinear crystal. A second harmonic pulse duration (FWHM) of 703 ps is measured. By assuming a Gaussian pulse shape, the inferred mid-IR pulse duration is 986 ns, as shown in Fig. 4(a). The pulse train was also measured using the same detector and is shown in Fig. 4(b). Finally, the output laser beam quality was characterized with a scanning slit beam profile analyzer (Ophir Photonics, NanoMode Scan). The collimated beam from the output of the amplifier was focused by a CaF_2 lens (f = 200 mm) along the optical axis of the instrument, and a M^2 value of 4.1 was obtained for both x and y axes. The value is lower than the theoretical maximum M^2 value of seven, derived from the fiber geometry (NA and core diameter) and output wavelength, indicating that the 0.12 NA of the amplifier fiber is not fully filled during pulse amplification.

We monitored the output power stability near 5 W over a 2 h period as shown in Fig. 5(a). Root-mean-square (RMS) fluctuations of 1.5% are obtained from this measurement. Normally, endcapping both the input and output fibers is required to protect the faces from OH degradation in long-term operation, as reported in [18]. In our case, since large multimode core sizes are already used, we did not notice any catastrophic damage of the fiber tips due to this phenomenon. A continuous power drop was observed over the first 20 min of amplifier operation before stabilization. The reason for such drop is associated with the pump coupling efficiency of the combiner, which reduces until the thermal steady state is obtained due to a large thermal expansion coefficient mismatch between fluoride and silica fibers in the combiner, as explained in [17]. To verify this hypothesis, the two combiners in the second amplification stage (PC3 and PC4) are tested separately at the same pump power level that was used for generating the 5 W output signal, and a similar power drop

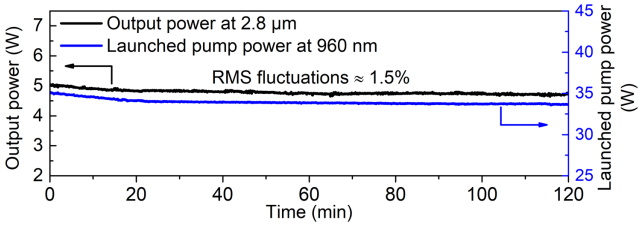

Fig. 5. (a) Evolution of the output power and (b) evolution of the total launched pump power near 5 W for a 120 min.

was observed for the total launched pump power from PC3 and PC4, as shown in Fig. 5(b).

The laser performance achieved in this work, in terms of output power, pulse energy, or pulse duration, is already more than appropriate for several applications related to biomaterial processing [5,19,20]. However, there is still a need for continued scaling, to achieve multi-mJ pulse energy and larger average power to enable efficient and fast cutting of hard tissues such as bone or tooth enamel [20]. To meet such requirements, several improvements must be realized. Most critical is the fiber material damage threshold. Although fluoride fibers have been less studied than fused silica fibers in that regard, one could estimate a damage threshold of 20 GW/cm^2 for our fluoride fibers at pulse durations near 1 ns [21]. This is to be compared to a value of 50 GW/cm^2 generally accepted for fused silica for such pulse duration [22]. The 1 mJ pulse produced here corresponds to an intensity of 10 GW/cm^2 at the output facet of the 115 μm core diameter fiber used in the second amplifier stage. This would leave room for a two-fold increase of pulse energy within the damage threshold. Clearly, a third amplification stage involving a larger fiber core would be required to further increase pulse energy, e.g., a 180 μm core would safely accommodate 5 mJ pulses. For optimal scaling to higher average power, it is important to manage the thermal load within the large core, highly doped gain fiber. Thus, it is critical to optimize the gain fiber's core/clad ratio and its doping concentration. Additionally, active cooling strategies could be employed to better extract the heat from the gain fiber. Another area of potential improvement is the optical isolator currently used between stages, which suffers from significant polarization sensitive losses. Ideally, the development of a mid-IR fiber coupled polarization insensitive isolator would enable monolithic architecture, leading to better seeding efficiencies between amplification stages. Our current optical isolator can safely handle average powers of 5 W, but this could be increased by a factor of two or three by scaling up the beam size accordingly for subsequent isolators to be placed between a second and third amplification stage. Regarding beam quality, one notes that large mode area gain fibers with reduced NA could be designed to reduce the M^2 of the output beam. Finally, as average power is increased further, dielectric coatings can be applied to the fiber tip as a diffusion barrier to prevent the process of OH-diffusion-induced photodegradation, as proposed in [18].

In conclusion, we demonstrated a high-energy fluoride fiber source operating near 3 μm based on the amplification in cascaded Er^{3+}:ZrF_4 fibers. The amplifier delivers 1 ns pulses at 5 kHz repetition rate with 1.02 mJ pulse energy. To the best of our knowledge, this is the first demonstration of a system combining high average power and mJ-level pulse energy together with short pulses based on a fluoride fiber. This amplifier clearly demonstrates that fluoride glass fibers have the potential to alleviate the great lack of compact and reliable sources of high-energy and short-pulse mid-IR laser pulses.

Funding. Mitacs (IT13672); Canada Foundation for Innovation (5180); Fonds de Recherche du Québec–Nature et Technologies (CO25665); Natural Sciences and Engineering Research Council of Canada (IRCPJ469414-1, RGPIN-2016-05877).

Acknowledgment. The authors thank Marc D'Auteuil and Stéphan Gagnon for technical assistance.

Disclosures. The authors declare no conflicts of interest.

Data Availability. Data underlying the results presented in this paper are not publicly available at this time but may be obtained from the authors upon reasonable request.

REFERENCES

1. C. Bader and I. Krejci, Am. J. Dent. **19**, 178 (2006).
2. S. Stübinger, C. Landes, O. Seitz, and R. Sader, J. Periodontol. **78**, 2389 (2007).
3. R. H. Kaufmann, A. Hartmann, and R. Hibst, J. Dermatol. Surg. Oncol. **20**, 112 (1994).
4. A. Böttcher, S. Kucher, R. Knecht, N. Jowett, P. Krötz, R. Reimer, U. Schumacher, S. Anders, A. Münscher, C. V. Dalchow, and R. D. Miller, Eur. Arch. Otorhinolaryngol. **272**, 941 (2015).
5. K. Franjic, M. L. Cowan, D. Kraemer, and R. J. D. Miller, Opt. Express **17**, 22937 (2009).
6. Y. O. Aydin, V. Fortin, R. Vallée, and M. Bernier, Opt. Lett. **43**, 4542 (2018).
7. Y. O. Aydin, V. Fortin, F. Maes, F. Jobin, S. D. Jackson, R. Vallée, and M. Bernier, Optica **4**, 235 (2017).
8. Y. Shen, Y. Wang, F. Zhu, L. Ma, L. Zhao, Z. Chen, H. Wang, C. Huang, K. Huang, and G. Feng, Opt. Lett. **46**, 1141 (2021).
9. X. Zhu, G. Zhu, C. Wei, L. V. Kotov, J. Wang, M. Tong, R. A. Norwood, and N. Peyghambarian, J. Opt. Soc. Am. B **34**, A15 (2017).
10. B.-M. Kim, M. D. Feit, A. M. Rubenchik, E. J. Joslin, J. Eichler, P. C. Stoller, and L. B. Da Silva, Appl. Phys. Lett. **76**, 4001 (2000).
11. X. Zhu and R. Jain, Opt. Lett. **33**, 1578 (2008).
12. H. Uehara, D. Konishi, K. Goya, R. Sahara, M. Murakami, and S. Tokita, Opt. Lett. **44**, 4777 (2019).
13. P. Wan, L.-M. Yang, S. Bai, and J. Liu, Opt. Express **23**, 9527 (2015).
14. Y. O. Aydin, V. Fortin, D. Kraemer, A. Fraser, R. Vallée, and M. Bernier, Opt. Lett. **43**, 2748 (2018).
15. W. Du, X. Xiao, Y. Cui, J. Nees, I. Jovanovic, and A. Galvanauskas, Opt. Lett. **45**, 5538 (2020).
16. N. Caron, M. Bernier, D. Faucher, and R. Vallée, Opt. Express **20**, 22188 (2012).
17. S. Magnan-Saucier, S. Duval, C. Matte-Breton, Y. O. Aydin, V. Fortin, S. LaRochelle, M. Bernier, and R. Vallée, Opt. Lett. **45**, 5828 (2020).
18. Y. O. Aydin, F. Maes, V. Fortin, S. T. Bah, R. Vallée, and M. Bernier, Opt. Express **27**, 20659 (2019).
19. L. Hänel, M. Kwiatkowski, L. Heikaus, and H. Schlüter, Futur. Sci. OA **5**, FSO373 (2019).
20. M. Hess, M. D. Hildebrandt, F. Müller, S. Kruber, P. Kroetz, U. Schumacher, R. Reimer, M. Kammal, K. Püschel, W. Wöllmer, and D. Miller, Eur. Arch. Otorhinolaryngol. **270**, 2927 (2013).
21. J.-C. Gauthier, V. Fortin, S. Duval, R. Vallée, and M. Bernier, Opt. Lett. **40**, 5247 (2015).
22. A.-C. Tien, S. Backus, H. Kapteyn, M. Murnane, and G. Mourou, Phys. Rev. Lett. **82**, 3883 (1999).